ACS APPLIED MATERIALS & INTERFACES

Research Article

www.acsami.org

Dry Self-Cleaning Properties of Hard and Soft Fibrillar Structures

Andrew G Gillies,*[,†] Jonathan Puthoff,[‡] Michael J Cohen,[§] Kellar Autumn,[‡] and Ronald S Fearing[⊥]

[†]Department of Mechanical Engineering, [§]Department of Materials Science and Engineering, and [⊥]Department of Electrical Engineering and Computer Science, University of California, Berkeley, California 94720, United States

[‡]Department of Biology, Lewis and Clark College, Portland, Oregon 97219, United States

ABSTRACT: Recently, gecko-inspired synthetic adhesives (GSAs) have been made using a variety of fabrication techniques and materials, with one made from a hard polymer having been reported to recover its shear adhesion after fouling by normal use, or "dry self-clean", a feature useful for applications in wall crawling robots, reusable adhesives, microfabrication and solar panel cleaning. This paper investigates the impact of two design parameters on the dry self-cleaning capability of GSAs by experimentally testing two GSAs after fouling with small (1 μm), medium (3−10 μm), and large (40−50 μm) particles. We found that a GSA made from a hard thermoplastic with nanoscopic fibers was able to recover 96−115% of its shear adhesion after fouling with small and large but not medium particles, while a GSA made from a soft polymer and microscopic fibers recovered 40−55% on medium and large particles, with SEM imaging revealing particles embedding within the polymer. An analysis of the contact strength between fibers, particles and substrates of various dimensions and elasticity reveals that dry self-cleaning will be more effective for GSAs fabricated with smaller fiber diameters and for GSAs fabricated from materials with smaller loss functions, such as hard thermoplastics. These results have important implications on the choice of materials and geometries used for GSAs when dry self-cleaning capability is a desired function in the material.

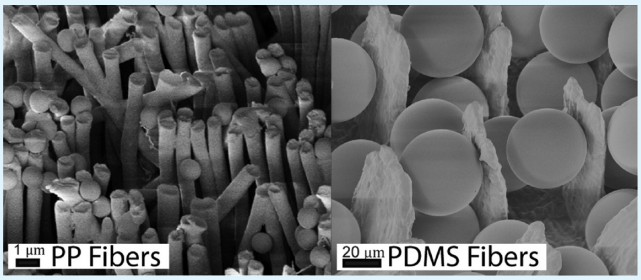

KEYWORDS: *gecko, adhesive, fibrillar, dry self-cleaning, particle contact, shear*

INTRODUCTION

Previous research on gecko feet has revealed that their amazing ability to climb vertically or inverted on nearly any surface can be attributed to van der Waals forces generated between the surface and millions of hierarchical nanohairs made from β-keratin (Young's modulus $\approx$ 1.5 GPa).[1,2] In addition, researchers have revealed that these hairs can shed dirt particles during use, keeping the adhesive pads clean enough to allow the gecko to continue climbing.[3] This dry self-cleaning effect has only been previously reported in natural gecko hairs and in polypropylene gecko-inspired synthetic adhesives.[4] This apparent ability to self-clean in dry environments is in contrast to the lotus effect, which requires droplets of water to shed particles from the highly hydrophobic surface.[5]

The ability of synthetic adhesives to dry self-clean during use would have many interesting applications such as in wall crawling robots, reusable adhesives, microfabrication and solar panel cleaning, and microparticle capture and control where other methods of particle control such as using water,[6,7] air jets,[8] electrostatics,[9] or other methods[10−12] are not sufficient.

Traditional pressure sensitive adhesives (PSA) are made using soft viscoelastic polymers (Young's modulus $\leq$100 kPa at 1 Hz[13,14]) that conform to a surface to achieve high adhesion. However, these soft polymers tend to foul quickly and lose their ability to adhere to a surface after several uses. Recently, gecko-inspired synthetic adhesives (GSAs)[15] have been made using a variety of fabrication techniques and materials. These adhesives generally consist of a surface covered in millions of micro- to nanoscopic fibers, the dimensions of which allow for the effective stiffness of the array to be reduced while maintaining morphological stability.[16] Structures can loosely be categorized into three types: soft polymers (Young's modulus $\leq$ 10 MPa)[17−22] hard polymers (Young's modulus $\approx$ 1 GPa)[23−27] and arrays of carbon nanotubes.[28−30] Autumn[31] has identified seven benchmark properties that are characteristic of geckolike adhesives, which are (1) anisotropic attachment, (2) a high adhesion coefficient, (3) a low detachment force, (4) material-independent adhesion, (5) self-cleaning, (6) antiself-adhesion, and (7) a nonsticky default state. Although several of the above-mentioned systems have shown one or more of these properties, only the hard polymer fibrillar arrays reported in Lee 2008[4] have shown the dry self-cleaning effect.

With the rapid advancement of many types of GSAs under way, it will be advantageous to understand the impact that the design parameters have on the dry self-cleaning effect discussed above. To date, no work has been done to directly compare what effect material choice or fiber diameter have on the dry self-cleaning property. This paper compares the dry self-cleaning capabilities of two example types of GSAs fabricated with different materials and dimensions; one made from a hard thermoplastic polymer (Young's modulus $\approx$ 1 GPa) with fiber

Received: March 6, 2013
Accepted: June 10, 2013
Published: June 10, 2013

 © 2013 American Chemical Society dx.doi.org/10.1021/am400839n | ACS Appl. Mater. Interfaces 2013, 5, 6081−6088

diameters ≈ 600 nm and the other made from a soft elastomer (Young's modulus ≤ 10 MPa) with fiber diameters ≈ 25 μm. Each type is subjected to a standard testing protocol across various particle sizes, which is used to quantify the cleaning effect through the establishment of an empirical recovery ratio, γ. An analysis of the contact strength between fibers, particles and substrates of various dimensions and elasticity is also carried out to explain the experimental findings and generalize the results.

Analysis: Self-Cleaning by Shear/Static Friction. Macroscopic friction forces are independent of the contact area between bodies, as described by Amontons' Law.[32] This is, however, not the case for microscopic, single-asperity contacts. In these cases, the static force required to produce interfacial sliding F_f is related to the strength of the interfacial bond in shear τ^* (a stress) and the contact area A, given by[33]

$$F_f = \tau^* A \tag{1}$$

Whether or not contacting bodies will slide relative to one another will be determined by the criterion $\tau \geq \tau^*$, where $\tau = F/A$ is the applied shear stress.

In problems with multiple, serial contacts (such as those incorporating a particle lodged between two surfaces) the sliding criterion will be different for each individual contact, because (i) the parameter τ^* depends on the properties of the materials involved and (ii) the applied stresses will vary with differing contact areas A. The interfacial shear strength of materials #1 and #2 can be estimated from their effective interfacial shear modulus G^* as[33]

$$\tau^* \approx \frac{G^*}{C} = \frac{1}{C}\left(\frac{2-\nu_1}{G_1} + \frac{2-\nu_2}{G_2}\right)^{-1} \tag{2}$$

where G_1, G_2, ν_1, and ν_2 are the shear moduli and Poisson's ratios of the different materials and $C \approx 25-30$ is an empirical factor relating the "yield stress" of the interface to the shear modulus. The other determining factor in the sliding criterion, the contact area between the bodies, will be in general unknown, although good solutions exist for the contact of spherical bodies under applied normal loading.[34,35] These contact areas will depend on the contact modulus $E^* \equiv [(1-\nu_1^2)/E_1 + (1-\nu_2^2)/E_2]^{-1}$, which includes the Young's moduli, E_1 and E_2, of the different materials.

The three-body contact problem for a contaminated fiber with a particle between itself and a substrate is shown in Figure 1. The fiber is pulled with transverse force F and imparts a normal load L to the particle. The triplets of elastic constants of the fiber, particle, and surface are, respectively, $\{E_f,G_f,\nu_f\}$, $\{E_p,G_p,\nu_p\}$, and $\{E_s,G_s,\nu_s\}$. Following Johnson–Kendall–Roberts (JKR) contact mechanics, there is a circular contact region between the particle and the surface with an area of[34]

$$A_{p,s} = \pi\left(\frac{3R_p}{4E^*_{p,s}}\right)^{2/3} \left(L + 3\pi\gamma R_p + \sqrt{6\pi\gamma R_p L + (3\pi\gamma R_p)^2}\right)^{2/3}, \tag{3}$$

where γ is the work of adhesion. The contact between the cylindrical fiber and the particle is a shape that is difficult to calculate, so here we assume it to be an ellipse whose semimajor axis is aligned with the axis of the fiber[36] and is equal to the JKR radius for the spherical case. If this ellipse has eccentricity e, then the area $A_{f,p}$ will be calculated in a similar manner to $A_{p,s}$ above, but will include an additional factor of $(1-e^2)$.

Using eqs 1, 2, and 3, we can determine the sliding criterion for the particle and the surface at all applied transverse forces F for fixed L = 250 nN and R_p = 500 nm. We assume a stiff particle (E_p = 10 GPa), a surface of intermediate modulus (E_s = 1 GPa), and that $\nu_p = \nu_s = 1/3$. The surface energy term γ is fixed at 0.05 J/m^2, typical for van der Waals interactions.[37] Similar calculations apply for the criterion for sliding between the fiber and the particle. We take R_f = 1000 nm, so e = 0.859. The resulting curves are in Figure 2. Sliding occurs at a lower threshold force for the fiber-particle system than for the particle-surface system, i.e., the fiber will self-clean under these conditions.

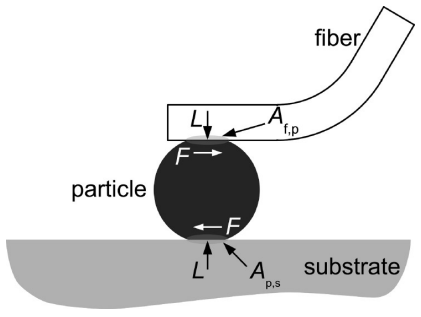

Figure 1. Schematic of fiber, contaminant particle, and substrate. The interfacial contact areas $A_{f,p}$ and $A_{p,s}$ depend on the materials properties and the normal load L. These areas and the applied lateral load F determine the shear stress acting at each interface.

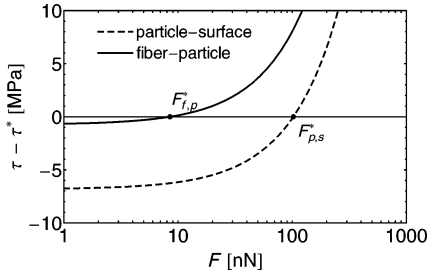

Figure 2. Sliding criteria for particle-surface and fiber-particle interfaces. The critical sliding forces for each contact are given by $F^*_{f,p}$ and $F^*_{p,s}$. For the given parameters, sliding threshold forces are smaller for the fiber-particle interface; this produces self-cleaning of the fiber.

The analysis above sets the threshold force for sliding at the i–j interface at $F^*_{i,j}$, as determined by the solutions to the curves in Figure 2. This is the force of static friction for the given interface and, in the case of a smooth or stick–slip mechanism, is required for sustained sliding.[33] We can explore how the different variables affect the cleaning properties of a fiber/particle/substrate system by defining a "cleaning parameter" ρ as

$$\rho \equiv \frac{F^*_{f,p}}{F^*_{p,s}} \tag{4}$$

When $\rho < 1$, sliding at the fiber-particle interface is favored and self-cleaning will be significant. When $\rho \approx 1$ or greater, self-cleaning is not expected to occur. Figure 3 shows how the

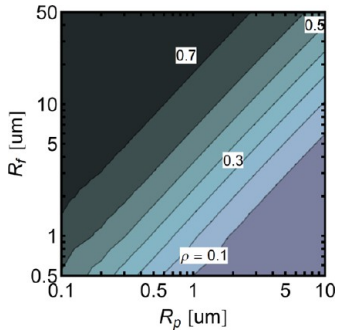

Figure 3. Cleaning parameter $\rho \equiv (F^*_{f,p}/F^*_{p,s})$ as determined by both fiber radius R_f and contaminant particle radius R_p. Self-cleaning by shear works best for small fibers and/or large particles.

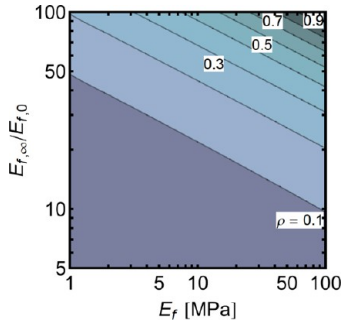

Figure 4. Cleaning parameter ρ for various combinations of fiber modulus E_f and intrinsic loss parameter $E_{f,\infty}/E_{f,0}$. Self-cleaning is poorest at high $E_{f,\infty}/E_{f,0}$.

cleaning parameter changes with both particle and fiber size. The data in Figure 3 indicate strong ($\rho \leq 0.77$) self-cleaning at all the $R_f - R_p$ combinations illustrated, though we note that, for combinations where $R_p \gg R_f$, up to n fibers may be associated with each contaminant particle. A straightforward modification of eq 4 to read $\rho \approx \beta(F^*_{f,p}/F^*_{p,s})$, where the arbitrary numerical parameter $\beta = \beta(n)$, can accommodate this additional detail.

The preceding analysis is a purely static one; we assume that the materials involved are perfectly elastic and exhibit no time-dependent behavior. This is not the case for real engineering materials, particularly those commonly in use in fibrillar adhesives such as PDMS, latex, and lightly cured urethane. In a dynamic picture of interfacial sliding, dissipative mechanisms will come into play and will affect the cleaning picture. Furthermore, deformation in individual fibers or wetting of contaminants can enhance the area of contact A.

Dissipation by internal relaxation mechanisms (viscous or plastic) will produce an effectively larger shear resistance τ^*_{eff}. The magnitude of the interfacial strength increase will depend on the dissipative properties of the material and the sliding velocity v,[38,39] so we write: $\tau^*_{eff} = \tau^*[1 + \Phi(\text{“lossiness”},v)]$. The form of the loss function Φ is a priori unknown, but it typically increases as the Young's moduli of the materials decrease and they become more rubberlike. Our measure of lossiness is the ratio of the short time-scale (or low-temperature) modulus E_∞ to the rubbery modulus E_0. Assuming a simple relationship like $\Phi = (E_\infty/E_0)\ f(v)$, where f is an unknown, dimensionless function of v, we have

$$\tau^*_{eff} = \tau^*\left[1 + \frac{E_\infty}{E_0} f(v)\right] \quad (5)$$

Figure 4 is an exploration of the $\{E_\infty/E_0, E\}$ parameter space for the fiber material. All the other material and geometrical properties are fixed at the values indicated for Figure 2, above. At fixed velocity, we take $f(v)$ = constant =10, for arguments sake. (In a quasi-static picture of frictional sliding, the v term is a representation of the strain rate in the materials.) An inspection of Figure 4 indicates that self-cleaning is inhibited at large values of $\{E_{f,\infty}/E_0, E_f\}$ and E_f.

MATERIALS AND METHODS

Polypropylene (PP) fibrillar surfaces were fabricated by molding a 12 μm thick polypropylene film into a 20 μm thick polycarbonate (PC) track-etched membrane filter (ISOPORE, Millipore Inc.) containing 600 nm diameter pores, as described previously,[40] and shown in Figure 5. The resulting fibers are 600 nm in diameter and 18 μm long, with a pitch of ≈1 μm. The resulting structures can been seen in Figure 7a.

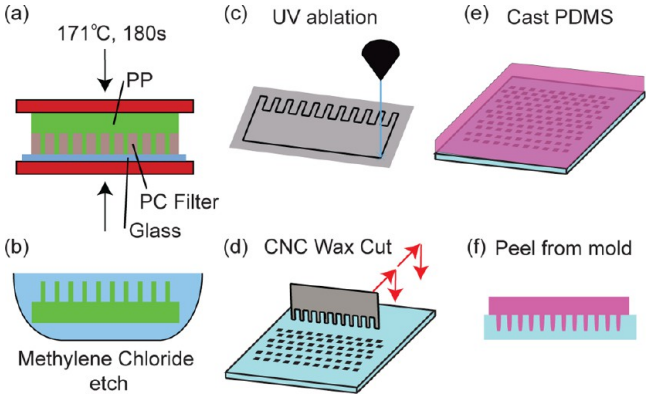

Figure 5. Fabrication of the PP and PDMS fibrillar structures. Polypropylene structures are made by (a) molding into a track-etched membrane filter in a hot press and then (b) etching away the filter with methylene chloride. PDMS structures are fabricated by first (c) cutting a 33 μm thick steel shim into a “comb” shape with a UV ablation laser, and (d) then with a CNC tool, the comb is used to make progressive cuts into a wax surface. (e) Once cut, PDMS is cast onto the wax mold and (f) released by peeling.

Polydimethylsiloxane (PDMS) (Sylgard 170, Dow Corning) fibrillar samples were manufactured by first fabricating a 33 μm thick steel shim into a 'comb' shape with a UV ablation laser, leaving comb dimensions of 25 μm wide teeth at the base, tapering to 15 μm at the tip, 70 μm in length, and a pitch of 40 μm. Then with a CNC tool, the comb is used to make progressive cuts into a wax surface.[41,42] Once cut, PDMS is cast onto the wax mold and the structures are released by peeling. The final fibers are 25 by 33 μm in diameter at the base, tapering to 15 × 33 μm at the tip, 70 μm tall, and spaced 40 μm apart. The resulting structures can been seen in Figure 7b.

The custom force displacement apparatus, shown in Figure 6a, is described in Gillies 2011.[40] Load-drag-pull step tests (Figure 6b) were performed on a custom built force displacement apparatus that mimics the methods used by Gravish[43] and Hansen,[3] which allows for a repeatable testing protocol. Samples are arranged in a loop to facilitate better contact with the surface, as well as to achieve some level of self-alignment.

The self-cleaning property of the GSAs were quantified with a protocol similar to that used by Hansen,[3] which consists of three stages. In stage one, pretraining of the GSAs was first measured by running nine samples of each type through 50 load-drag-pull steps on clean glass in order to pretrain the fibers. In stage two, samples were stepped across a clean glass slide 40 times, each step in a new location that would act as a benchmark for the self-cleaning steps. In the third stage, the samples are fouled (described below) and then stepped across the same 40 locations used in the benchmark stage so that a

dx.doi.org/10.1021/am400839n | ACS Appl. Mater. Interfaces 2013, 5, 6081−6088

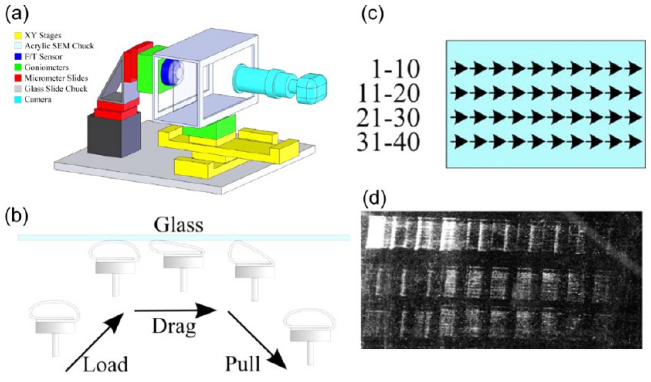

Figure 6. (a) Force displacement apparatus block diagram. (b) Load-drag-pull step on glass surface. (c) Spacing of steps after fouling to avoid stepping in contaminated areas of the glass slide. (d) Particles shed on glass after successive steps with a fouled PP fibrillar sample.

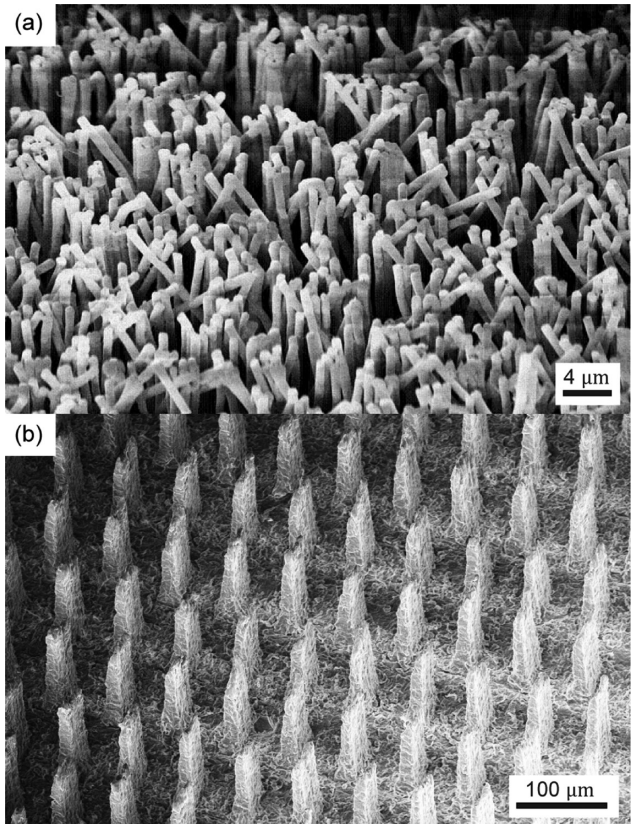

Figure 7. (a) Unused clean fabricated polypropylene fibrillar surface. (b) Unused clean fabricated PDMS fibrillar surface.

direct comparison of the adhesive properties before and after the fouling can be made independent of local substrate conditions.

Fouling of the PP and the PDMS samples was performed by taking a single LDP step on a glass slide coated in one of three types of fouling agents, referred to as small (1 μm polystyrene microspheres), medium (3–10 μm glass microspheres) and large (40–50 μm glass microspheres) particles.

RESULTS

Polypropylene Fibrillar Structure. Figure 8a shows an example of a load-drag-pull step of a PP sample before fouling. Stress on the *Y*-axis is calculated by dividing the measured force by the estimated microfiber contact area, determined from in situ observations obtained with a camera, using frustrated total

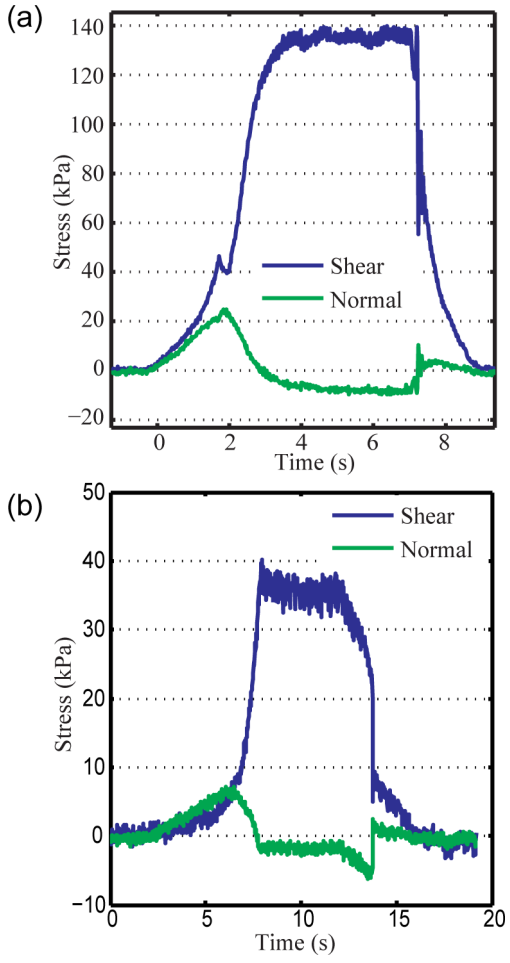

Figure 8. Typical load–drag–pull step for: (a) polypropylene fiber sample on a clean glass substrate, (b) PDMS fiber sample on a clean glass substrate.

internal reflection at the interface of the side-illuminated glass substrate and the microfiber array.[44] During the drag a high shear stress of ≈140 kPa is measured, whereas the normal stress goes from a compressive state during loading into a slight tensile stress during the drag phase indicating that shear adhesion is taking place, a behavior typical of GSAs.

To measure the effect of fouling on the samples, a recovery ratio is defined as $\gamma = (F_{\text{dirt\_}n})/(F_{\text{clean\_}n})$, where $F_{\text{dirt\_}n}$ is the maximum shear force during the recovery step n and $F_{\text{clean\_n}}$ is the maximum shear force from the benchmark step n. Figure 9 shows the recovery ratio for the PP fibrillar samples for 40 steps following the fouling step for the small, medium and large particles. Samples recovered 96 ± 11% of their initial shear adhesion within 10–15 steps on the glass when fouled with small particles, and recovered 115 ± 12% of their shear adhesion when fouled with large particles. The increase in shear adhesion beyond the initial trials is likely due to fibers continuing to 'train' after the fouling step, as reported by Lee.[45] However samples fouled with medium sized particles only recovered 36 ± 20%. During the self-cleaning steps, particles were left on the glass by the samples, as seen in Figure 6d, with the amount of particles left on the glass from each subsequent step decreasing, indicating that the majority of the particles are removed from the sample onto the glass in the first several steps. This was observed with all particle sizes.

dx.doi.org/10.1021/am400839n | ACS Appl. Mater. Interfaces 2013, 5, 6081–6088

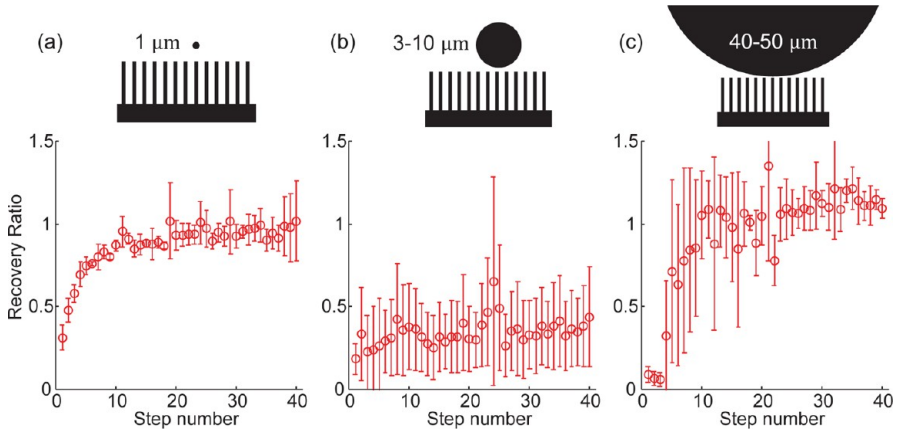

Figure 9. Shear recovery ratio $\gamma = F_{dirt\_n}/F_{clean\_n}$ for the polypropylene fibrillar surface after fouling with (a) small (mean = 96 ± 11%), (b) medium (mean = 36 ± 20%), and (c) large particles (mean = 115 ± 12%). (N = 3 samples for each particle type, error bars are ± S.D.).

Figure 10 shows the PP structures 40 steps after fouling with (a) 1 μm polystyrene spheres, (b) 3−10 μm glass spheres and (c) 40−50 μm glass spheres. After the 40 cleaning steps, fibers in the contact zone appear to have shed a majority of the 1 μm PS spheres, however, some spheres can still be seen on the fibers, adhering to the sides of the fibers below the tips, with others still remaining on top. However, fibers contaminated with 3−10 μm glass spheres still have spheres in the contact zone, some being deeply embedded between the fibers. Of the fibers fouled with 40−50 μm glass spheres, only a single glass sphere could be found on the sample after the 40 cleaning steps.

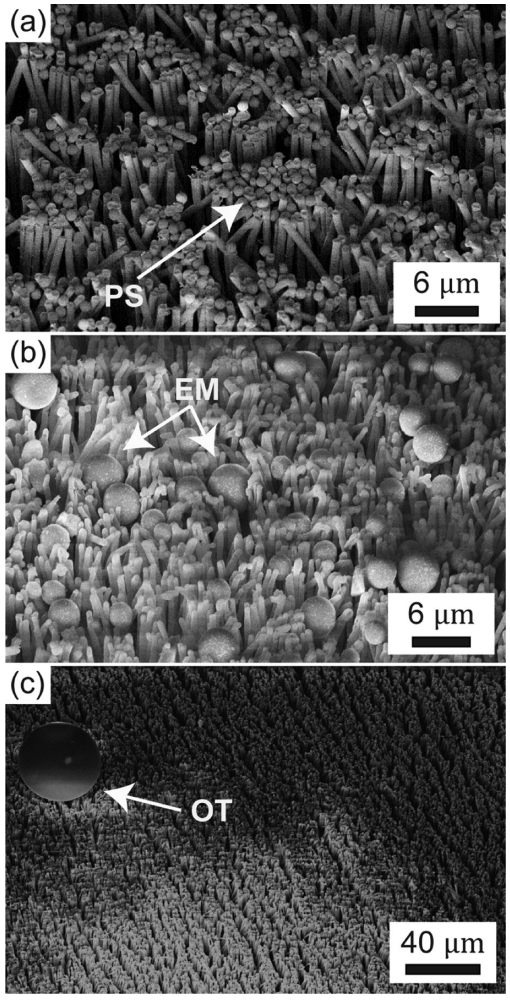

Figure 10. (a) Polypropylene fibrillar structures 40 steps after fouling with 1 μm polystyrene spheres, which can be seen between fibers (PS); (b) fibers fouled with 3−10 μm glass spheres, where some can be seen deeply embedded (EM) between fibers, and (c) fibers contaminated with 40−50 μm glass spheres, only one of which could be found sitting on top (OT) on the sample 40 steps after fouling.

Polydimethylsiloxane Fibrillar Structure. Figure 8b shows an example of a load-drag-pull step of a PDMS sample before fouling. Stress on the Y-axis is calculated as described for the PP fiber samples. From the plot we can see a similar behavior to the PP sample, indicating that shear adhesion of ≈40 kPa is taking place under a slight tensile load. This is less shear adhesion than the PP samples, but is still performing well for a soft polymer GSA.

Recovery from fouling of the PDMS samples was calculated the same as for the PP samples, using the recovery ratio, γ. Figure 11 shows the recovery ratio for the PDMS fibrillar samples for 40 steps following the fouling step for the small, medium, and large particles. When fouled with small particles, PDMS fibers recovered 99 ± 4% of initial shear adhesion; however, no particles could be seen deposited on the glass during the recovery steps. When fouled with medium and large-sized particles, PDMS samples lost 40 ± 15% and 55 ± 18% of their initial shear adhesion, respectively.

Figure 12 shows the PDMS structures 40 steps after fouling with (a) 1 μm polystyrene spheres, (b) 3−10 μm glass spheres, and (c) 40−50 μm glass spheres. After the 40 cleaning steps, 1 μm PS spheres can be seen deeply embedded within the fiber tips, almost to the point of being "absorbed" by the PDMS. Fibers contaminated with 3−10 μm glass spheres are still coated in particles after 40 recovery steps. Fibers coated with 40−50 μm glass spheres are also still covered in particles, showing particles embedded between the fibers after the 40 cleaning steps.

DISCUSSION

The results indicate that the fouling particle size has a large impact on the self-cleaning properties of the two GSAs. In general, our experimental results are consistent with our analytical prediction that harder fibrillar structures with nanoscale dimensions will dry self-clean more readily than softer fibrillar structures with microscale dimensions. This is

dx.doi.org/10.1021/am400839n | ACS Appl. Mater. Interfaces 2013, 5, 6081−6088

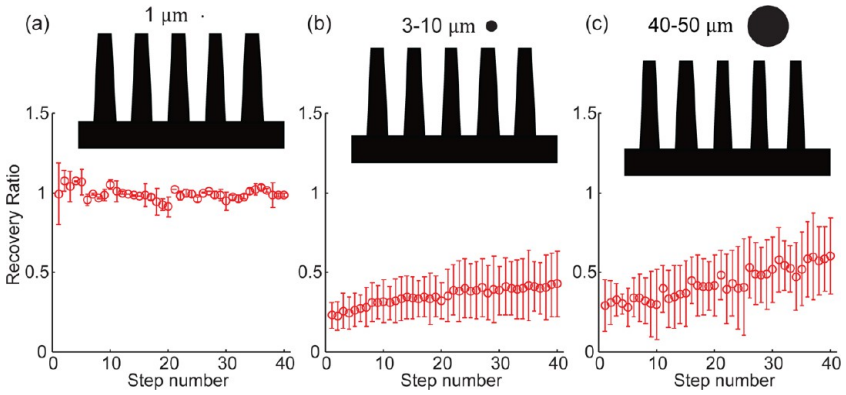

Figure 11. Shear recovery ratio $\gamma = F_{dirt\_n}/F_{clean\_n}$ for the PDMS fibrillar surface after fouling with (a) small (mean=99 ± 4%), (b) medium (mean = 40 ± 15%), and (c) large particles (mean = 55 ± 18%). (N = 3 samples for each particle type, error bars are ± S.D.).

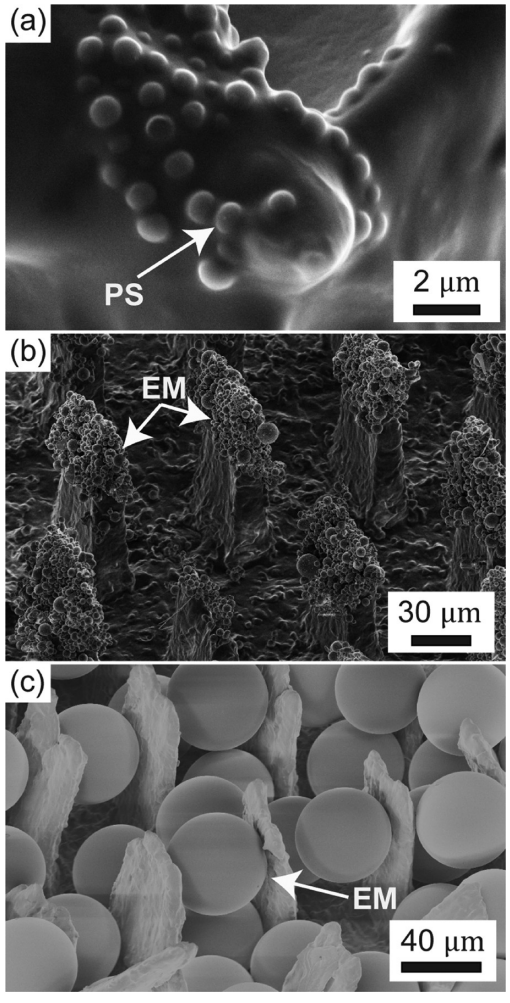

Figure 12. (a) PDMS fibrillar structures 40 steps after fouling with 1 μm polystyrene spheres, which can be seen deeply embedded in the fiber tips (PS). (b) Fibers fouled with 3−10 μm glass spheres, where many particles can be seen embedded on the outside of the fibers (EM) (c) Fibers contaminated with 40−50 μm glass spheres after 40 recovery steps. Particles can be readily seen embedded between the fibers (EM).

evidenced by SEM images showing particles releasing from the PP structures, while becoming deeply embedded in the PDMS structures. As well, a comparison of the empirical recovery ratio between the two GSA types across the various particle sizes (Figure 13) reveals that the harder PP structures dry self-clean across a wider range of particle sizes, and that larger particles

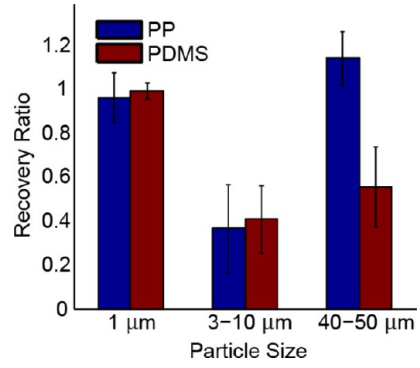

Figure 13. Comparison of the PP and PDMS fiber structures dry-self-cleaning recovery ratio across the various particle sizes tested.

more readily self-clean. These results are supported by the analysis, as seen in Figure 3, which shows that smaller fibers and larger particles are more likely to self-clean. The analysis also predicts that materials with a higher loss modulus (Figures 4 and 5) are less likely to self-clean, which is also found in the experimental data in Figure 13. From this, we can state a general design rule that to maximize adhesion while avoiding fouling, structures with low loss functions, $E_{f,\infty}/E_{f,0}$, and smaller fiber diameters, R_f, are favored.

However, we have observed two phenomena in our experimental data that cannot be explained by our analysis. Namely, the inability of the PP structures to recover from medium sized particles, despite particles observed on the glass substrate after recovery steps, and that PDMS fibers do not lose adhesion from small particle contamination, despite particles found deeply embedded in the fiber tips after the recovery steps. This indicates that there may be several mechanisms in operation that are still not understood.

For the first phenomenon, SEM images of the PP structures after recovery from medium particle fouling reveal 3−8 μm particles embedded near the surface of the array. Unlike the 1 μm PS particles seen between the fibers after recovery, these particles are large enough to disrupt the contact of the fibers with the substrate, preventing them from adhering. We postulate that an intermediate range of particles exists for which they are small enough to fit between the fibers, but large enough to disrupt contact. Once the fibers are too large to

become embedded between fibers, they will preferentially shed to the substrate, as seen with the larger 40−50 μm particles. Because our analysis does not consider fibrillar spacing, this experimental observation is not captured.

For the second phenomenon, we observe deep embedding of the 1 μm sphere within the PDMS fiber (Figure 12a) almost as if the sphere is being absorbed. It could be the case that the PDMS fiber is so soft, and the particle so small that the fiber is able to wrap around the small particle and still make contact with the surface. This type of large deformation is beyond the scope of the analysis, and therefore would not be captured. It is also possible that the PS spheres are so small that they too aid in adhesion by acting as small contact points, or spatulae, increasing contact with the glass.

Furthermore, removal of particles from the fibers to the surface may not be the only mechanism by which the samples are recovering adhesion. PS microspheres seen on the SEM image of the PP sample after cleaning indicate that recovery is occurring despite their presence. It is possible some particles are pushed down between the fibers, away from the surface where they were first interfering with the fibers. Also, it is possible that some particles are being removed to the substrate during the lifting phase, in the normal direction, instead of being cleaned in shearing. As well, large clumps of particles at the trailing edge of the contact zone indicate that fibers are being brushed backward off the sample. This may be why the loop geometry is able to recover much more shear adhesion than the 30% recovery reported by Lee.[4] The loop structure gives a shorter path along which the particles can escape, as opposed to the long flaps used previously by Lee.[4]

CONCLUSION

The ability of gecko-inspired synthetic adhesives to dry self-clean during use has many potential interesting applications such as in wall crawling robots, reusable adhesives, microfabrication and solar panel cleaning and microparticle capture and control where other methods of particle control are not sufficient. We have investigated the impact of two design parameters on the dry self-cleaning capability of GSAs by experimentally testing two GSAs after fouling with small (1 μm), medium (3−10 μm) and large (40−50 μm) particles. We found that a GSA made from a hard thermoplastic with nanoscopic fibers was able to recover 96−115% of its shear adhesion after fouling with small and large but not medium particles, while a GSA made from a soft polymer and microscopic fibers recovered 40−55% on medium and large particles. Further examination by SEM revealed that the PDMS structures were not shedding the smaller particles during recovery steps, but were instead being absorbed into the surface, and that, regardless of their size, particles did not release from the PDMS surface. An analysis of the contact strength between fibers, particles and substrates of various dimensions and elasticity reveals that dry self-cleaning will be more effective for GSAs fabricated with smaller fiber diameters and for GSAs fabricated from materials with smaller loss functions, such as hard thermoplastics. This has important implications on the choice of materials and geometries used for GSAs when dry self-cleaning capability is a desired function in the material, and indicates that hard polymer GSAs with smaller fiber diameters are less prone to fouling.

AUTHOR INFORMATION

Corresponding Author

*E-mail: andrew.gillies@berkeley.edu.

Notes

The authors declare no competing financial interest.

ACKNOWLEDGMENTS

The authors thank Brian Bush for SEM imaging, Bryan Schubert for process assistance, and the Biomimetic Millisystems Lab for their support. This work was supported by NSF CMMI Grant 0856789.

REFERENCES

(1) Autumn, K.; Sitti, M.; Liang, Y. A.; Peattie, A. M.; Hansen, W. R.; Sponberg, S.; Kenny, T. W.; Fearing, R. S.; Israelachvili, J. N.; Full, R. J. *Proc. Natl. Acad. Sci.* **2002**, *99*, 12252−6.
(2) Autumn, K.; Majidi, C.; Groff, R. E.; Dittmore, A.; Fearing, R. S. *J. Exp. Biol.* **2006**, *209*, 3558−68.
(3) Hansen, W. R.; Autumn, K. *Proc. Natl. Acad. Sci.* **2005**, *102*, 385−9.
(4) Lee, J.; Fearing, R. S. *Langmuir* **2008**, *24*, 10587−91.
(5) Barthlott, W.; Neinhuis, C. *Planta* **1997**, *202*, 1−8.
(6) Tsai, Y.-C.; Shih, P.-J.; Lin, T.-H.; Shih, W.-P. *2006 1st IEEE International Conference on Nano/Micro Engineered and Molecular Systems*; IEEE: Piscataway, NJ, 2006; pp 1388−1391.
(7) Zhang, X.; Kong, B.; Tsui, O. K. C.; Yang, X.; Mi, Y.; Chan, C. M.; Xu, B. *J. Chem. Phys.* **2007**, *127*, 014703.
(8) Otani, Y.; Namiki, N.; Emi, H. *Aerosol Sci. Technol.* **1995**, *23*, 665−673.
(9) Desai, A.; Lee, S.; Tai, Y. *Sens. Actuators, A* **1999**, *73*, 37−44.
(10) Haake, A.; Dual, J. *Ultrasonics* **2004**, *42*, 75−80.
(11) Vehring, R.; Aardahl, C. L.; Davis, E. J.; Schweiger, G.; Covert, D. S. *Rev. Sci. Instrum.* **1997**, *68*, 70.
(12) Donovan, R. P. *Particle Control for Semiconductor Manufacturing* Marcel Dekker: New York, 1990; p 464.
(13) Dahlquist, C. A. In *Treatise on Adhesion and Adhesives*; Patrick, R. L., Ed.; Marcel Dekker: New York, 1969; Vol. *2*, pp 219−260.
(14) Pocius, A. V. *Adhesion and Adhesive Technology*; Hanser: Munich, Germany, 2002; pp 43−77.
(15) Autumn, K.; Gravish, N. *Philos. Trans. R. Soc. London, Ser. A* **2008**, *366*, 1575−90.
(16) Spolenak, R.; Gorb, S.; Arzt, E. *Acta Biomater.* **2005**, *1*, 5−13.
(17) Sitti, M.; Fearing, R. S. *J. Adhes. Sci. Technol.* **2003**, *17*, 1055−1073.
(18) Varenberg, M.; Gorb, S. *J. R. Soc., Interface* **2007**, *4*, 721−5.
(19) Kim, S.; Aksak, B.; Sitti, M. *Appl. Phys. Lett.* **2007**, *91*, 221913.
(20) Murphy, M. P.; Aksak, B.; Sitti, M. *Small* **2009**, *5*, 170−5.
(21) Glassmaker, N. J.; Jagota, A.; Hui, C.-Y.; Noderer, W. L.; Chaudhury, M. K. *Proc. Natl. Acad. Sci.* **2007**, *104*, 10786−91.
(22) Parness, A.; Soto, D.; Esparza, N.; Gravish, N.; Wilkinson, M.; Autumn, K.; Cutkosky, M. *J. R. Soc., Interface* **2009**, *6*, 1223−32.
(23) Zhang, Y.; Lo, C.-W.; Taylor, J. A.; Yang, S. *Langmuir* **2006**, *22*, 8595−601.
(24) Geim, A. K.; Dubonos, S. V.; Grigorieva, I. V.; Novoselov, K. S.; Zhukov, A. A.; Shapoval, S. Y. *Nat. Mater.* **2003**, *2*, 461−3.
(25) Kustandi, T.; Samper, V.; Yi, D.; Ng, W.; Neuzil, P.; Sun, W. *Adv. Funct. Mater.* **2007**, *17*, 2211−2218.
(26) Schubert, B.; Lee, J.; Majidi, C.; Fearing, R. S. *J. R. Soc., Interface* **2008**, *5*, 845−53.
(27) Jeong, H. E.; Lee, J.-K.; Kim, H. N.; Moon, S. H.; Suh, K. Y. *Proc. Natl. Acad. Sci.* **2009**, *106*, 5639−44.
(28) Yurdumakan, B.; Raravikar, N. R.; Ajayan, P. M.; Dhinojwala, A. *Chem. Commun.* **2005**, 3799−801.
(29) Ge, L.; Sethi, S.; Ci, L.; Ajayan, P. M.; Dhinojwala, A. *Proc. Natl. Acad. Sci.* **2007**, *104*, 10792−5.
(30) Qu, L.; Dai, L. *Adv. Mater.* **2007**, *19*, 3844−3849.

(31) Smith, A. M.; Callow, J. A.; Autumn, K. In *Biological Adhesives*; Smith, A. M., Callow, J. A., Eds.; Springer: Berlin, 2006; pp 225−255.
(32) Bhushan, B. *Introduction to Tribology*, 1st ed.; John Wiley & Sons: New York, 2002.
(33) Carpick, R. W.; Enachescu, M.; Ogletree, D. F.; Salmeron, M. *Mater. Res. Soc. Symp. Proc.* **1999**, *539*, 93−103.
(34) Johnson, K. L.; Kendall, K.; Roberts, A. D. *Proc. R. Soc. London, Ser. A* **1971**, *324*, 301−313.
(35) Derjaguin, B. V.; Muller, V. M.; Toporov, Y. P. *J. Colloid Interface Sci.* **1975**, *53*, 314−326.
(36) Hrouz, J.; Vojta, V.; Ilavský, M. *Polym. Eng. Sci.* **1980**, *20*, 402−405.
(37) Israelachvili, J. *Intermolecular and Surface Forces*, 2nd ed.; Harcourt Brace and Co.: London, U.K., 1991; p 204.
(38) Puthoff, J. B.; Prowse, M. S.; Wilkinson, M.; Autumn, K. *J. Exp. Biol.* **2010**, *213*, 3699−3704.
(39) Momozono, S.; Nakamura, K.; Kyogoku, K. *J. Chem. Phys.* **2010**, *132*, 114105.
(40) Gillies, A. G.; Fearing, R. S. *Langmuir* **2011**, *27*, 11278−11281.
(41) Gillies, A. G.; Kwak, J.; Fearing, R. S. *Adv. Funct. Mater.* **2013**.
(42) Day, P.; Eason, E. V.; Esparza, N.; Christensen, D.; Cutkosky, M. *J. Micro and Nano-Manuf.* **2013**, *1*, 1−10.
(43) Gravish, N.; Wilkinson, M.; Autumn, K. *J. R. Soc., Interface* **2008**, *5*, 339−48.
(44) Lee, J.; Majidi, C.; Schubert, B.; Fearing, R. S. *J. R. Soc., Interface* **2008**, *5*, 835−844.
(45) Lee, J.; Fearing, R. S.; Komvopoulos, K. *Appl. Phys. Lett.* **2008**, *93*, 191910.